Supporting Information

Synergistic Regulation of Dual Monomers for Constructing High Bandgap and High Polarity Polyimide with High-Temperature Capacitive Energy Storage Performance

Chuanjia Jiao[1,2], Jiayan Li[1,2], Caixia Wan[3], Jiawei Zou[1,*], Shifang Luan[1,2,*]

1 State Key Laboratory of Polymer Science and Technology, Changchun Institute of Applied Chemistry, Chinese Academy of Sciences, Changchun 130022, China

2 School of Applied Chemistry and Engineering, University of Science and Technology of China, Hefei 230026, China

3 National Synchrotron Radiation Laboratory, University of Science and Technology of China, Hefei 230029, China

Corresponding Author:

jwzou@ciac.ac.cn; sfluan@ciac.ac.cn

Characterization:

The Fourier infrared spectroscopy (FT-IR) curves were measured on a Bruker alpha. The UV-vis spectra were measured on a PerkinElmer Lambda3S, Fluorescence spectra were measured by using a research grade FLSP 920 fluorescence spectrometer (Edinburgh Instruments, UK). Thermal gravimetric analyzer (TGA) curves were carried out on a Mettler Toledo TGA2 with a heating rate of 10 °C/min under a nitrogen atmosphere. Differential Scanning Calorimetry curves were carried on a TA DSC Q2000 with a heating rate of 10 °C/min under a nitrogen atmosphere. First, the temperature was raised from 50 °C to 250-400 °C, held for 5 minutes, and then cooled back to 50 °C at the same rate to eliminate the thermal history. Finally, the temperature was increased again to 250-400 °C, and the second heating data was used to determine the glass transition temperature. XRD tests were performed using Brucker D8 ADVANCE. with measuring angle from 5 ° to 70 °, equipped with a Cu Kα source (λ = 1.54 Å). Mechanical properties of the specimens were characterized on an Instron 5869 universal testing machine (Instron, USA) at a strain rate of 20 mm/min. Prior to electrical testing, copper (Cu) electrodes were deposited on both surfaces of the PI films via thermal evaporation. For the measurement of electric displacement–electric field (*D*-*E*) loops and dielectric breakdown strength, circular electrodes with a diameter of 3.4 mm were used, corresponding to an effective area of 9.08 mm^2. For the measurement of leakage currents, direct current conductivity, and thermally stimulated depolarization current (TSDC) profiles, electrodes with a diameter of 7 mm were employed, providing an effective area of 38.48 mm^2. Dielectric properties were performed through an Agilent LCR instrument (4294A). Electric displacement electric field (*D*-*E*) loops were obtained by PolyK (PK CPE20B) using a modified Sawyer-Tower circuit, in which the dielectric films were exposed to a triangular unipolar wave at a frequency of 100 Hz. Dielectric breakdown strength was recorded on a Trek 610C at a voltage rise rate of 500 V/s. The experiment was conducted in a silicone oil bath to reduce surface corona discharge. The leakage currents, direct current conductivity, and TSDC profiles were evaluated using an electrometer (Keithley 6517A). The leakage

current was collected with an electric field gradient of 25 MV/m. The TSDC characterization procedures are as follows: after a 30-minute polarization at 250 °C and rapid cooling to -10 °C for minutes, the specimens were short-circuited, and the current was recorded as the temperature increased from -10 to 250 °C with the heating rate of 5 °C/min.

Density functional theory (DFT) calculation:

Amorphous cells were constructed using Materials Studio (MS) software, with each cell containing 5 molecular chains and a polymerization degree of 12. Molecular dynamics simulations were performed on the amorphous cells of all polymers under isothermal (NVT) and isoenergetic equilibration (NVE) conditions, and at least five annealing processes were applied to each. Density functional theory (DFT) calculations were conducted using the Materials Studio (MS). The electron exchange and correlation energy were treated within the generalized gradient approximation (GGA) with the Perdew-Burke-Ernzerhof (PBE) functional, and a plane-wave basis set with a cutoff energy of 500 eV was employed. The energy calculation and geometry optimization were terminated when the electronic energy tolerance reached 1×10^{-5} eV/atom and the maximum force component on any atom was less than 0.02 eV/Å, respectively. The band gap of the materials was determined by calculating the highest occupied molecular orbital (HOMO) and lowest unoccupied molecular orbital (LUMO) from the density of states. To account for van der Waals interactions, the empirical correction from the Grimme scheme (DFT-D3) was adopted, and the charge density difference was visualized using VMD software. Additionally, the Gaussian16 package was used to optimize the geometric structures of different polymer molecules at the B3LYP/6-31G* level of theory in a vacuum, and the wavefunction results were analyzed using Multiwfn software.

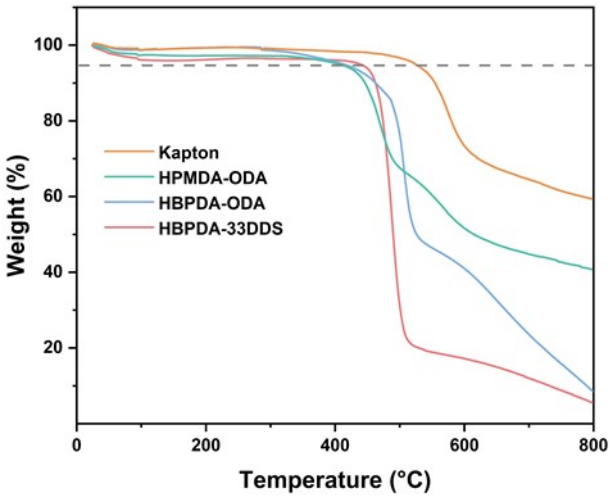

Fig. S1. Thermal gravimetric analysis curves of Kapton, HPMDA-ODA, HBPDA-ODA and HBPDA-33DDS.

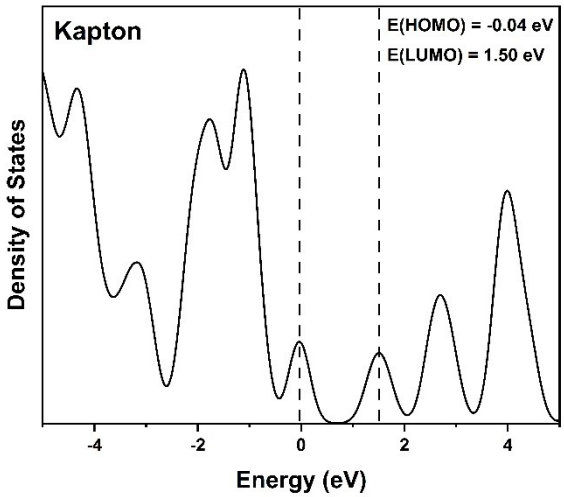

Fig. S2. The results of the density of states (DOS) calculations for Kapton.

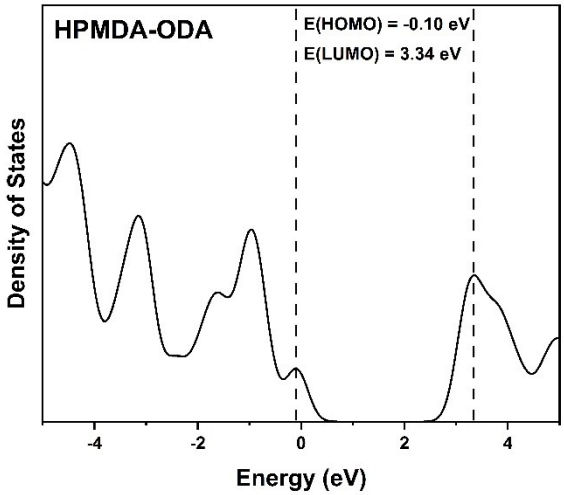

Fig. S3. The results of the density of states (DOS) calculations for HPMDA-ODA.

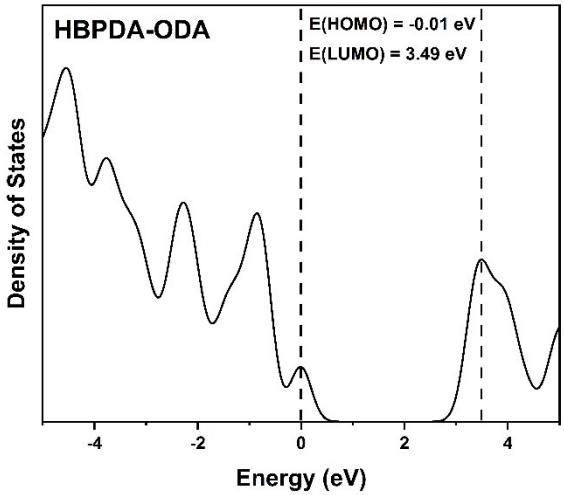

Fig. S4. The results of the density of states (DOS) calculations for HBPDA-ODA.

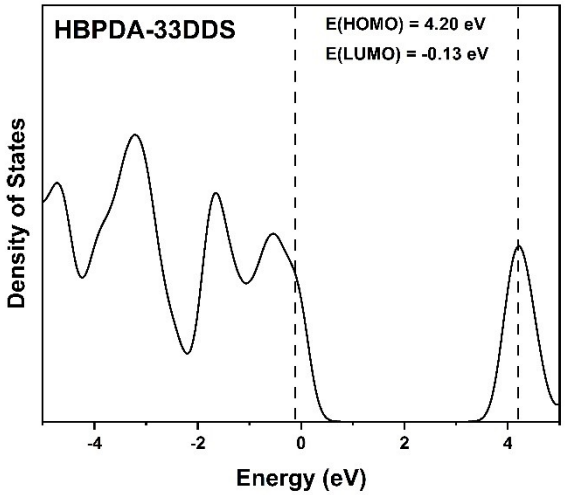

Fig. S5. The results of the density of states (DOS) calculations for HBPDA-33DDS.

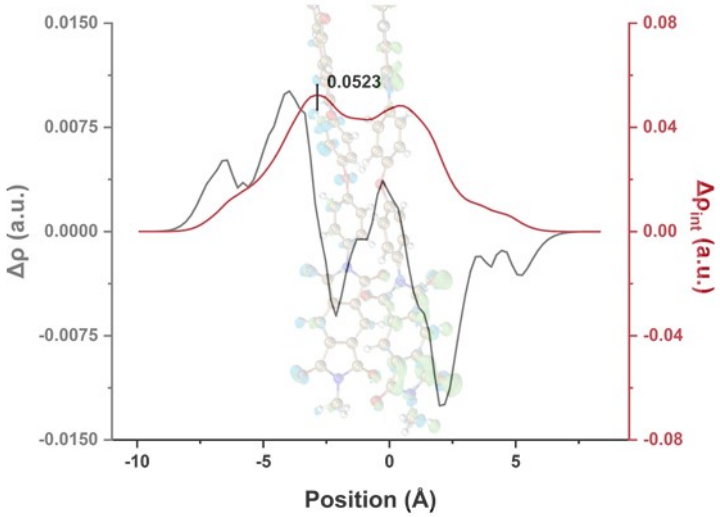

Fig. S6. The differential charge densities of Kapton before and after applying an electric field of 400 MV/m.

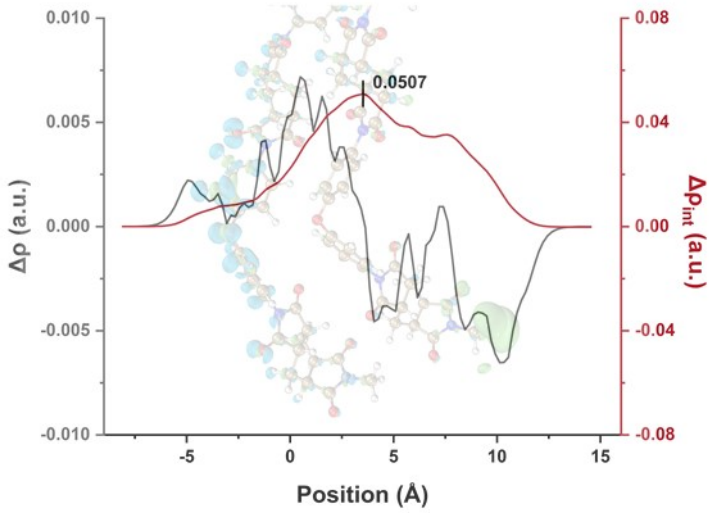

Fig. S7. The differential charge densities of HPMDA-ODA before and after applying an electric field of 400 MV/m.

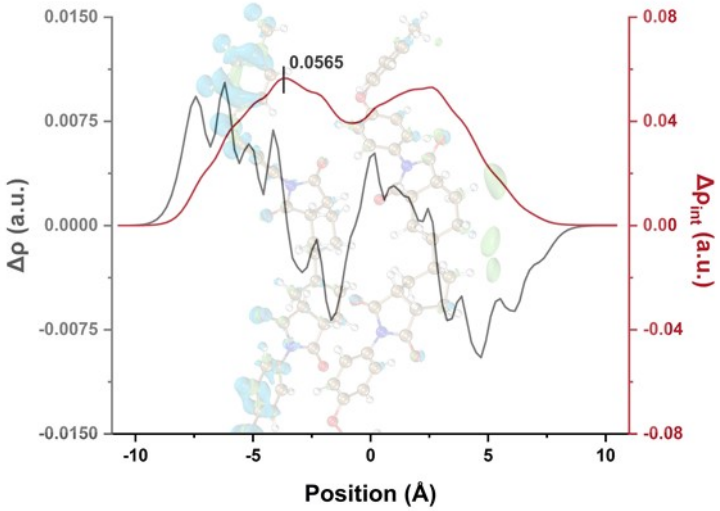

Fig. S8. The differential charge densities of HBPDA-ODA before and after applying an electric field of 400 MV/m.

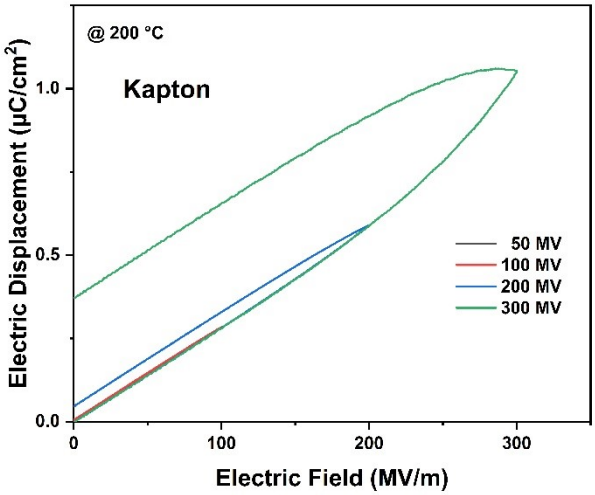

Fig. S9. Electric displacement electric field (D-E) loops of Kapton at 200 °C and 100 Hz.

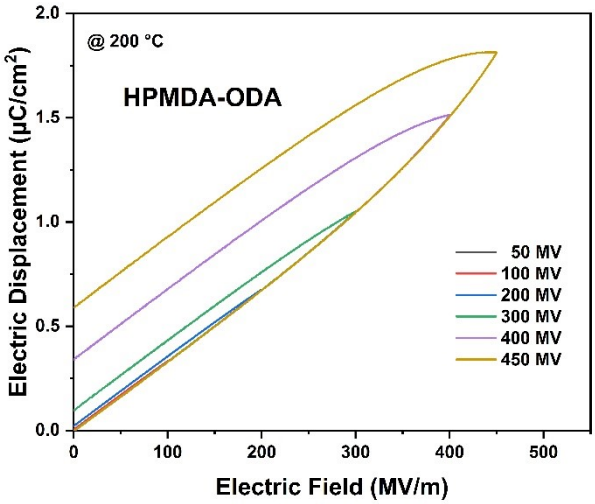

Fig. S10. Electric displacement electric field (D-E) loops of HPMDA-ODA at 200 °C and 100 Hz.

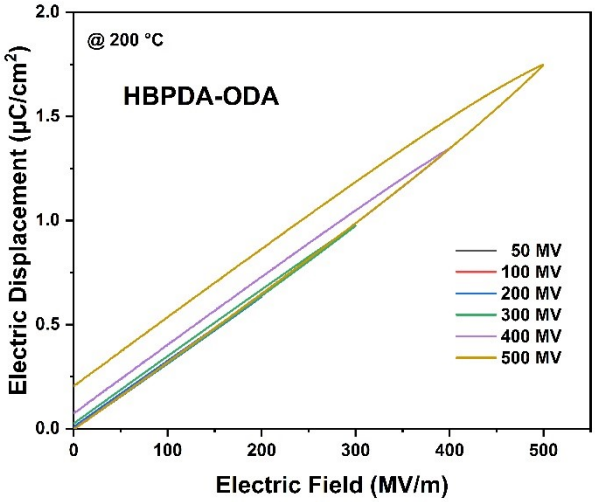

Fig. S11. Electric displacement electric field (D-E) loops of HBPDA-ODA at 200 °C and 100 Hz.

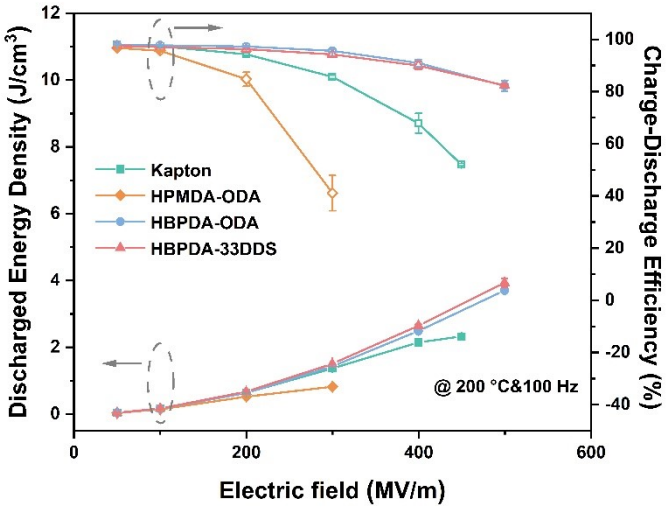

Fig. S12. Energy storage density and charge–discharge efficiency of the tested films at 200 °C and 100 Hz. Data points and error bars represent the mean values and standard deviations calculated from at least three independent samples, respectively.

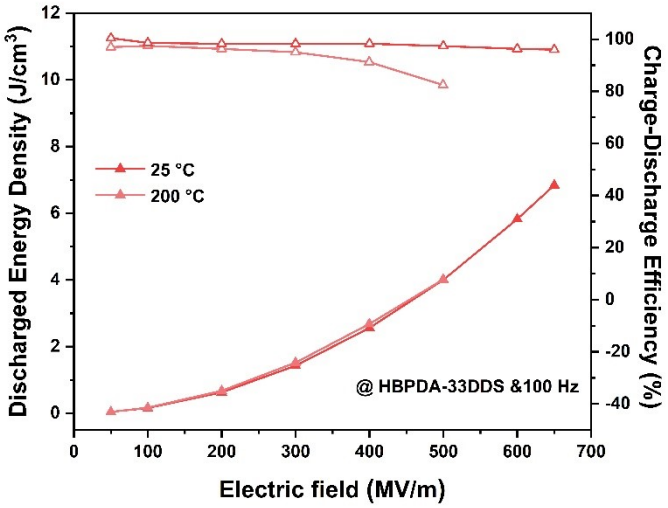

Fig. S13. Discharged energy density and charge-discharge efficiency of HBPDA-33DDS at 25 °C and 200 °C (100 Hz).

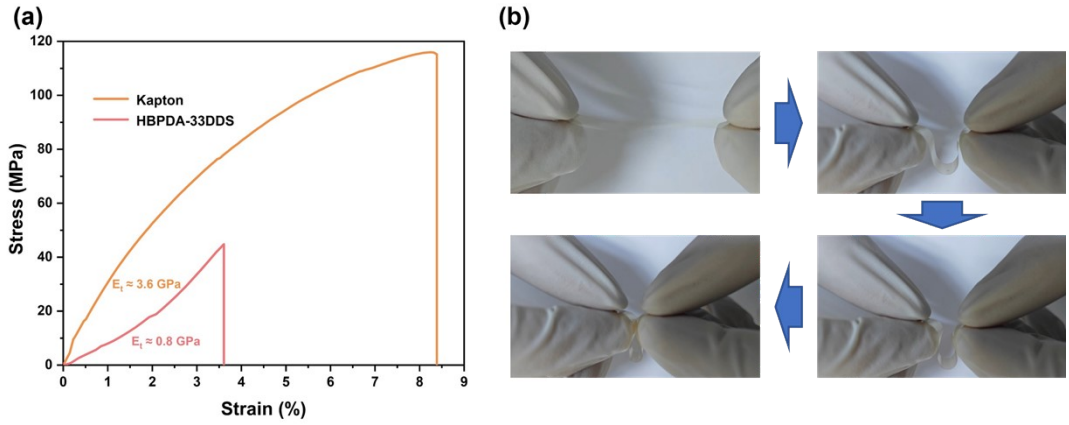

Fig. S14. Mechanical properties and flexibility of the polyimide films. (a) Tensile stress–strain curves of the commercial Kapton and synthesized HBPDA-33DDS films. (b) Digital photographs demonstrating the flexibility and structural integrity of the standalone HBPDA-33DDS film under manual bending and stretching.